



UNIVERSIDADE FEDERAL DO PARÁ
INSTITUTO DE GEOCIÊNCIAS
PROGRAMA DE PÓS-GRADUAÇÃO EM GEOFÍSICA

DISSERTAÇÃO DE MESTRADO

**1D CMP inversion of MCSEM data to create a 3D
geoelectrical model**

JORLIVAN LOPES CORRÊA

Belém
2017

JORLIVAN LOPES CORRÊA

1D CMP inversion of MCSEM data to create a 3D geoelectrical model

Dissertação apresentada ao Programa de Pós-Graduação
em Geofísica da Universidade Federal do Pará para obtenção
do título de Mestre em Geofísica.

Área de Concentração: Métodos Eletromagnéticos

Orientador: Prof. Dr. Cícero Roberto Teixeira Régis

Belém
2017

Dados Internacionais de Catalogação de Publicação (CIP)
Biblioteca do Instituto de Geociências/SIBI/UFPA

Corrêa, Jorlivan Lopes, 1989-

1D CMP inversion of MCSEM data to create a 3D
geoelectrical model / Jorlivan Lopes Corrêa. – 2017.

22 f. : il. ; 30 cm

Inclui bibliografias

Orientador: Cícero Roberto Teixeira Régis

Dissertação (Mestrado) – Universidade Federal do Pará,
Instituto de Geociências, Programa de Pós-Graduação em
Geofísica, Belém, 2017.

1. Inversion (Geophysics). 2. Prospecting - Geophysical
methods. 3. Petroleum – Prospecting. I. Título.

CDD 22. ed. 550

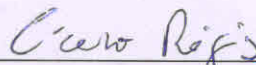
JORLIVAN LOPES CORRÊA

1D CMP inversion of MCSEM data to create a 3D geoelectrical
model

Dissertação apresentada ao Programa de Pós-Graduação em
Geofísica do Instituto de Geociências da Universidade Fede-
ral do Pará, como requisito final para obtenção do título de
Mestre em Geofísica.

Data de aprovação: 06 de abril de 2017

Banca Examinadora:



Cícero Roberto Teixeira Régis – Orientador.
Doutor em Geofísica
Universidade Federal do Pará



Emanuel José Capechi de Pinho
Doutor em Física
Petrobras



Marcos Welby Correa Silva
Doutor em Geofísica
Universidade Federal do Pará

Dedico esta dissertação a Deus pela saúde e energia para a realização do trabalho, a minha esposa e meu filho pela motivação e a meus pais pelo sacrifício com que me trouxeram até aqui.

AGRADECIMENTOS

Ao professor Cícero Roberto Teixeira Régis pela orientação. Ao corpo docente e ao administrativo do Programa de Pós-Graduação em Geofísica da UFPA. À Petrobras, pelo uso dos recursos computacionais. Ao colega Marcos Malmann Medeiros pela ajuda na elaboração de figuras. À banca examinadora pelas sugestões, que de fato melhoraram o trabalho.

RESUMO

Neste trabalho é apresentada a aplicação da aproximação CMP (Common Mid Point–distancia média entre fonte e receptor) de dados CSEM a uma inversão 1D neste domínio de forma a gerar como resultado um cubo de resistividades. As aquisições CSEM são 3D, com uma malha de receptores. Sendo assim, distribuimos os dados no domínio CMP para que toda a região do grid de inversão tenha algum dado. Para que tenhamos solução estável nesse processo é utilizado o regularizador de suavidade nas 3 direções, de modo que o resultado traz um sentido geológico que espera variações suaves de resistividade em subsuperfície. O processo é implementado de maneira que todas as células de cada coluna CMP façam parte do mesmo vetor de parâmetros a ser determinado. O modelo de resistividade utilizado como teste tem características 3D com variações laterais do corpo anômalo e gerou uma resposta satisfatória para o estudo.

Palavras-chaves: MCSEM. Inversão eletromagnética 1D. CMP.

ABSTRACT

This work presents the application of 1D inversion of marine CSEM data in the CMP (Common Mid Point) approximation to generate a cube of resistivities. The method is applied to data from 3D surveys. An interpretive model is build in the form of columns of homogeneous zones which form a 3D resistivity grid. The data is distributed in the CMP domain so that each resistivity column in the inversion grid contains some data points. To achieve a stable solution the smoothing regularizer is applied in all 3 directions, so that the generated geological models present smooth variations in the resistivity. The method is successfully applied to a set of synthetic data generated from a 3D model which includes two resistive targets at different depths.

Keywords: MCSEM. 1D electromagnetic inversion. CMP.

LISTA DE FIGURAS

2.1	Acquisition configurations. Triangles represent receivers. The transmitters are assumed to be over the appropriate receiver positions in each source-receiver pair.	2
2.2	CMP column.	3
2.3	One CMP data. The color represent the different receivers, the gaps are the distance between the receivers, 1 Km	3
3.1	Test model: 1.5 km water layer with $0.3 \Omega\cdot\text{m}$, background with $1\Omega\cdot\text{m}$ and target with $100\Omega\cdot\text{m}$	7
3.2	Acquisition layout for the simulated survey.	8
3.3	Slice XZ plane on 0 m on Y.	9
3.4	Slice YZ plane on -2500 m on X.	9
3.5	Slice YZ plane on -5500 m on X.	10
3.6	Depth slice on 2220 m.	10
3.7	Depth slice on 3150 m.	11
3.8	misfit	11
3.9	Misfit maps for the 3 frequencies used in the example.	12
3.10	Slice XZ plane on 0 m on Y.	13
3.11	Slice YZ plane on -2400 m on X.	14
3.12	Slice YZ plane on -5500 m on X.	14
3.13	Depth slice on 2450 m.	15
3.14	Depth slice on 3450 m.	15
3.15	Model 2: 1.5 km water layer over layered sediments and a resistive target with $100\Omega\cdot\text{m}$	17
3.16	Slice XZ plane on 0 m on Y.	18
3.17	Slice YZ plane on 0 m on X.	18
3.18	Depth slice on $z = 2500$ m.	19
3.19	Misfit maps for the 3 frequencies used in the example.	20

SUMÁRIO

1	INTRODUCTION	1
2	METHOD	2
3	APPLICATION TO SYNTHETIC DATA	6
3.1	MODEL 1	6
3.1.1	Start model	6
3.1.2	CSEM data	6
3.1.3	Inversion results	6
3.1.4	Simulation of well constraint	13
3.2	MODEL 2	16
3.2.1	Inversion results 2	16
4	FINAL REMARKS	21
	REFERENCES	22

1 INTRODUCTION

The Marine Controlled Source Electromagnetic (mCSEM) method's rise in oil exploration since the 2000's brought forth an efficient tool to mapping resistive targets, with good lateral definition (Buonora et al., 2014; Barker and Baltar, 2016). Inversion of mCSEM data remains a challenging task, especially if one needs to resolve 3D structures, which demands a great amount of computer resources. In many applications, some computer time can be saved by choosing a suitable initial model for the inversion. Starting with a homogeneous model is a common practice, but if a reasonable approximation to the resistivity under the survey lines can be built prior to the inversion, then convergence may be achieved with less iterations.

Mittet et al. (2008) presented a 1D inversion scheme using the Common MidPoint (CMP) gathers approximation which was able to recover 2D structures. In that method, the data for the 1D inversions are composed of measurements from all source-receiver offsets in the 2D survey that share the same common midpoint, and a separate 1D inversion is performed for each CMP. This method was improved by Crepaldi et al. (2011) with the introduction of analytical derivatives to calculate sensitivities, which made the process significantly faster, and lateral constraints (Dell'Aversana and Vivier, 2009; Tseng et al., 2012; MacGregor and Tomlinson, 2014) to allow the inversion of a CMP data set to influence the results of the surrounding CMPs, which improved the approximation achieved to the true 2D structures.

The same approach, with analytical derivatives and lateral constraints, is applied here to invert data from 3D surveys. The design of a 3D survey allows the data on a single CMP to be composed of source-receiver pairs from multiple survey lines and multiple directions, therefore increasing the amount of information used in each 1D inversion. Each CMP generates a column of resistivities which are used to build a 3D "cube", representing the volume underneath the survey area.

The results show that the method can achieve a sufficiently good approximation to allow a preliminary 3D interpretation, and to generate an approximate 3D model to be used as first guess in a true 3D inversion.

2 METHOD

The data are acquired in configurations that allow multiple source-receiver pairs to contribute to each 1D inversion for each CMP, as illustrated in figure 2.1.

The observed data are the horizontal components of the electric field (E_x, E_y), represented as the vector \mathbf{d} ; the parameter vector is \mathbf{m} , formed by the N_p values of the logarithms of the resistivities of each homogeneous layer in each CMP column (figure 2.2); the mathematical model of the synthetic data as a function of the parameters is $\mathbf{F}(\mathbf{m})$, which represents the layered Earth response calculated as shown in Crepaldi et al. (2011).

To achieve stable solutions, minimum gradient (smoothing) constraints are implemented between adjacent parameters in both vertical and lateral directions. The vertical constraints are necessary to regularize each CMP inversion, whereas the horizontal constraints are used to allow the inversion of each CMP to exert influence on the results of its surrounding columns. This lateral smoothing usually carries more weight in the process than the vertical smoothing, because in geological environments sharper variations are expected in the vertical than in the horizontal direction. The implementation also allows for leaving some parameters unconstrained, to account for situations where discontinuities are expected, such as in the borders of salt or igneous intrusions.

The application of Occam's inversion (Constable et al., 1987) generates a smooth model as an approximation to the real earth in the sense that it is able to generate synthetic data that fit the observations. The smoothing constraints are introduced through the

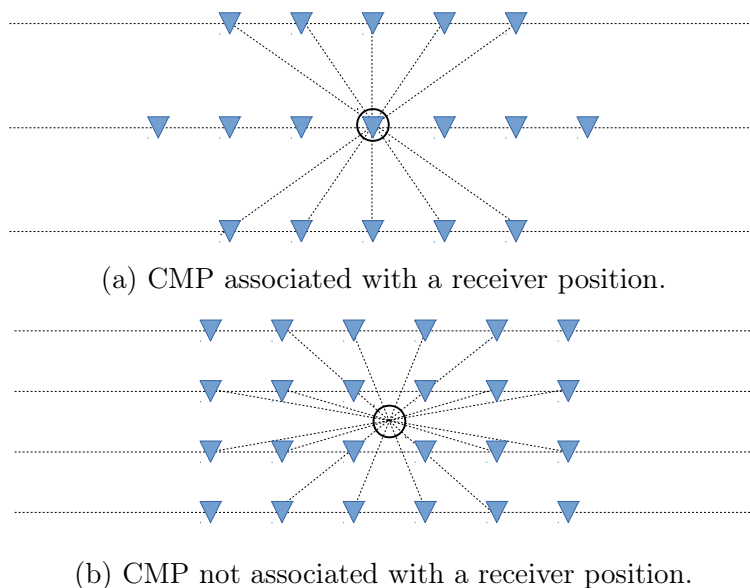


Figure 2.1: Acquisition configurations. Triangles represent receivers. The transmitters are assumed to be over the appropriate receiver positions in each source-receiver pair.

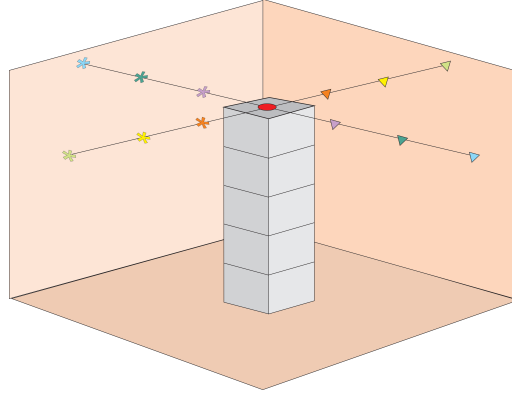


Figure 2.2: CMP column.

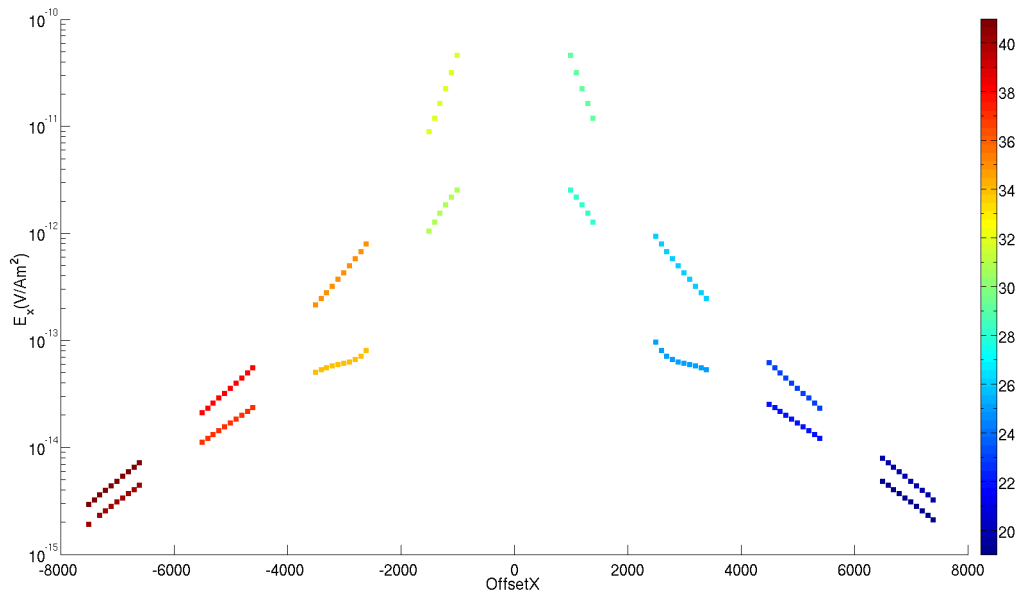


Figure 2.3: One CMP data. The color represent the different receivers, the gaps are the distance between the receivers, 1 Km

matrices $\mathbf{S}_{(x,y,z)}$. Each row of a smoothing matrix defines which parameters are to be constrained to each other, simply by placing a -1 and a 1 in the positions corresponding to those parameters, and leaving zeroes in the remaining elements. When this matrix is applied to the parameter vector \mathbf{m} in the functional to be minimized, it has the effect of imposing that the difference between those two parameters is as small as possible, by enforcing that the equation

$$\mathbf{S}\mathbf{m} = \mathbf{0} \quad (2.1)$$

be satisfied in a least squares sense.

Another kind of *a priori* information may be included through the use of absolute equality constraints (Medeiros and Silva, 1996), which are useful when reliable information exists about the resistivities in a given set of parameters, as when there is well logging data in the region under the survey. In this case, if there are N_c parameters to be constrained, the method defines a vector \mathbf{m}_p , with only the N_c values to be attributed from the *a priori* information, and a matrix $\mathbf{P}_{N_c \times N_p}$, each row of which has a value of 1 in the the position corresponding to the parameter to be constrained and zeroes elsewhere, such that

$$\mathbf{P}\mathbf{m} = \mathbf{m}_p. \quad (2.2)$$

In the inversion process, the equalities imposed by the constraint matrices (equations 2.1 and 2.2) are enforced in a least squares sense.

The functional to be minimized, then, includes a term for fitting the data, and one for each kind of constraint that enters the process. It is written as

$$\begin{aligned} \phi = & [\mathbf{d} - \mathbf{F}(\mathbf{m})] \mathbf{W}_d [\mathbf{d} - \mathbf{F}(\mathbf{m})] + a_H (\mathbf{m}^T \mathbf{S}_x^T \mathbf{W}_x \mathbf{S}_x \mathbf{m} + \mathbf{m}^T \mathbf{S}_y^T \mathbf{W}_y \mathbf{S}_y \mathbf{m}) \\ & + a_V (\mathbf{m}^T \mathbf{S}_z^T \mathbf{W}_z \mathbf{S}_z \mathbf{m}) + a_p (\mathbf{P}\mathbf{m} - \mathbf{m}_p)^T W_p (\mathbf{P}\mathbf{m} - \mathbf{m}_p). \end{aligned} \quad (2.3)$$

In this functional, the regularization parameters a set the relative weighting for the different constraints. The matrix \mathbf{W}_d is defined as a function of the uncertainties in the measurements, such as the standard deviations associated with each measurement. The method also allows the use of weighting matrices ($\mathbf{W}_{(x,y,z,p)}$) to define different degrees of constraining to different regions of the interpretive models.

The inversion is an implementation of Gauss-Newton, with the Levenberg-Marquardt method (Marquardt, 1963; Auken and Christiansen, 2004), in which in each iteration the damping parameter μ is multiplied or divided by a factor based on the success of the previous generated model. The inicial Marquardt damping parameter is 10 and the multiplicative factor is 2.

In the k^{th} iteration the regularized estimator is, then, written as

$$m_{k+1} = m_k + [J_k^T W_d J_k + a_H(S_x^T W_x S_x + S_y^T W_y S_y) + a_V(S_z^T W_z S_z) + a_p W_p + \mu I]^{-1} [(W_d J_k)^T (d - F(m_k)) + a_H(S_x^T W_x S_x m_k + S_y^T W_y S_y m_k) + a_V(S_z^T W_z S_z m_k) + a_p W_p (m_k - m_p)], \quad (2.4)$$

where the elements of the Jacobian matrix \mathbf{J} are the sensitivities:

$$J_{ij} = \frac{\partial \log |E_i|}{\partial \log(\rho_j)}. \quad (2.5)$$

Here, the logarithms are employed to reduce the range of values of the field amplitudes and resistivities, which can span several orders of magnitude. The logarithms also have the advantages of damping the amplification the short offsets and preventing negative values to be attributed to the resistivities.

To take advantage of the analytical derivatives of the field, the sensitivities, as defined in equation 2.5, are calculated as

$$J_{ij} = \frac{\rho_j}{|E_i|^2} Re \left\{ E_i^* \frac{\partial E_i}{\partial \rho_j} \right\}. \quad (2.6)$$

The iteration represented by equation 2.4 is repeated until the convergence criteria are satisfied. In this application, the stopping criteria are the minimum variation of the model, the minimum variation of data misfit and the minimum misfit. As a non convergence criterium, the process also stops after a specified number of iterations is achieved.

3 APPLICATION TO SYNTHETIC DATA

This chapter presents two example applications of the method to synthetic data sets.

3.1 MODEL 1

In the first example, we invert synthetic data generated by the 3D model shown in figure 3.1. Two 100 m thick resistive targets (100 Ohm-m) are embedded in a conductive (1 Ohm-m) host, under a 1,500 m thick water layer. The first target is a T shaped body placed at 1,500 m below the sea bed; the second is a slab at a depth of 2,500 m below the sea bed. The model covers a total area of 160 km². The survey configuration (figure 3.2) has 9 receiver lines, and 7 source lines running at 50 m above the flat sea bed. The receiver lines are equally spaced, with a separation of 2,000 m. Each has 21 receivers spaced by 1 km. The source lines extend from 10 km to the left of the first receiver to 10 km to the right of the last receiver. The source lines are between x coordinates -6000 m and 6000 m. In each source line, the sources are simulated at 100 m intervals.

The 3D forward model calculation of the synthetic observations was based on the integral equation method presented by Zhdanov (2009). Data were generated at three frequencies (0.25, 0.75 and 1.25 Hz).

3.1.1 Start model

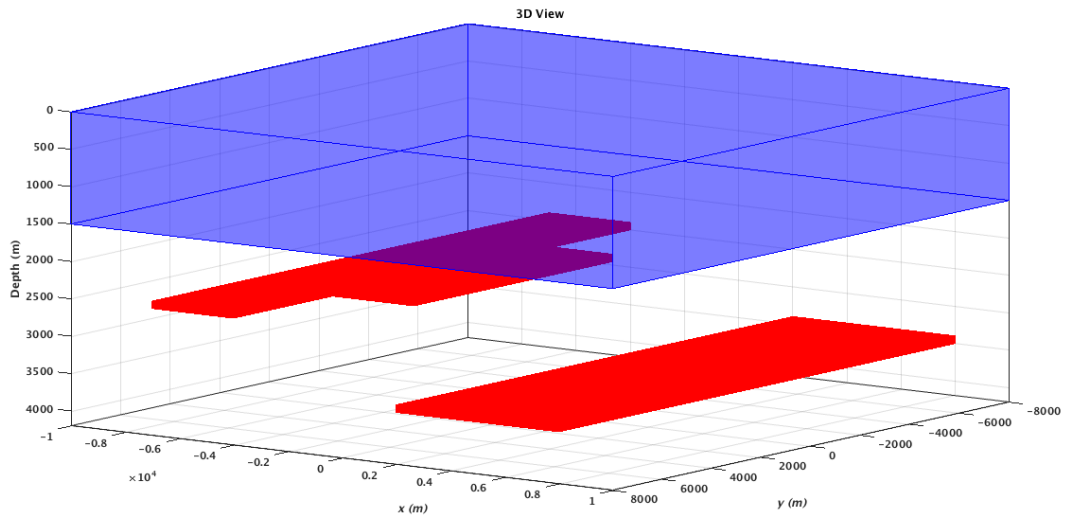
The interpretive model is formed by a 410 column grid in with 41×10 cells in the xy plane, each a 500 m by 1500 m rectangle. The first layer is 25 m thick. Thicknesses of the inversion layers increase with with depth by a factor of 1%, to compensate for the decrease in sensitivity with depth. The starting model is homogeneous, all layers start at a resistivity of 1 Ohm-m.

3.1.2 CSEM data

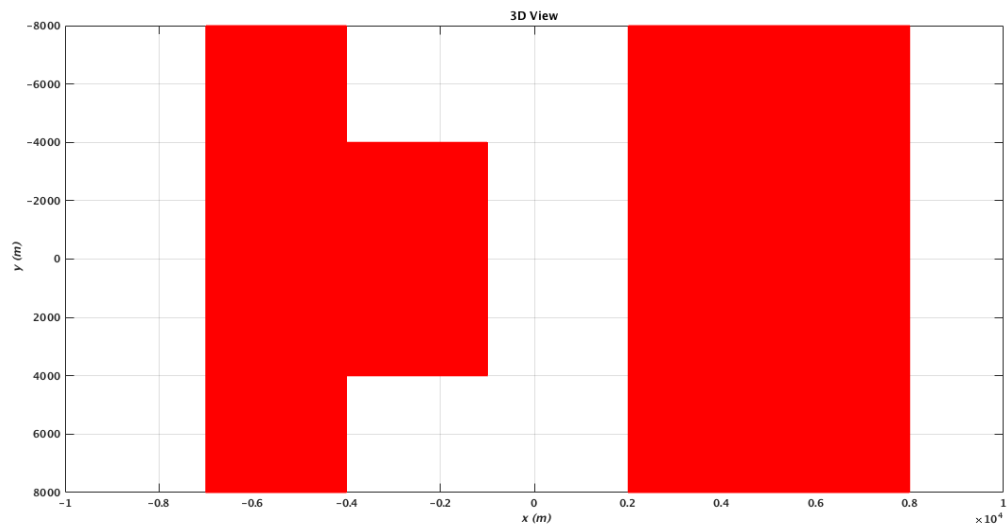
The synthetic data were contaminated with 3% gaussian noise. For the inline E_x field, offsets ranging from 1 km to 10 km were used. For the broadside E_x component, the used offsets were from 1 km to 8 km. The cutoff of the data is at the amplitude of 10^{-15} V/Am². For the E_y data, offsets between 1 km and 5 km were used.

3.1.3 Inversion results

Figures 3.3 to 3.9 show the results of inverting the data without any absolute equality constraints. The smoothness regularization weights for the horizontal constraints is 0.1, and the one for the vertical constraints is 0.05. These parameters were chosen as



(a) 3D model view.



(b) Top view.

Figure 3.1: Test model: 1.5 km water layer with $0.3 \Omega \cdot \text{m}$, background with $1 \Omega \cdot \text{m}$ and target with $100 \Omega \cdot \text{m}$.

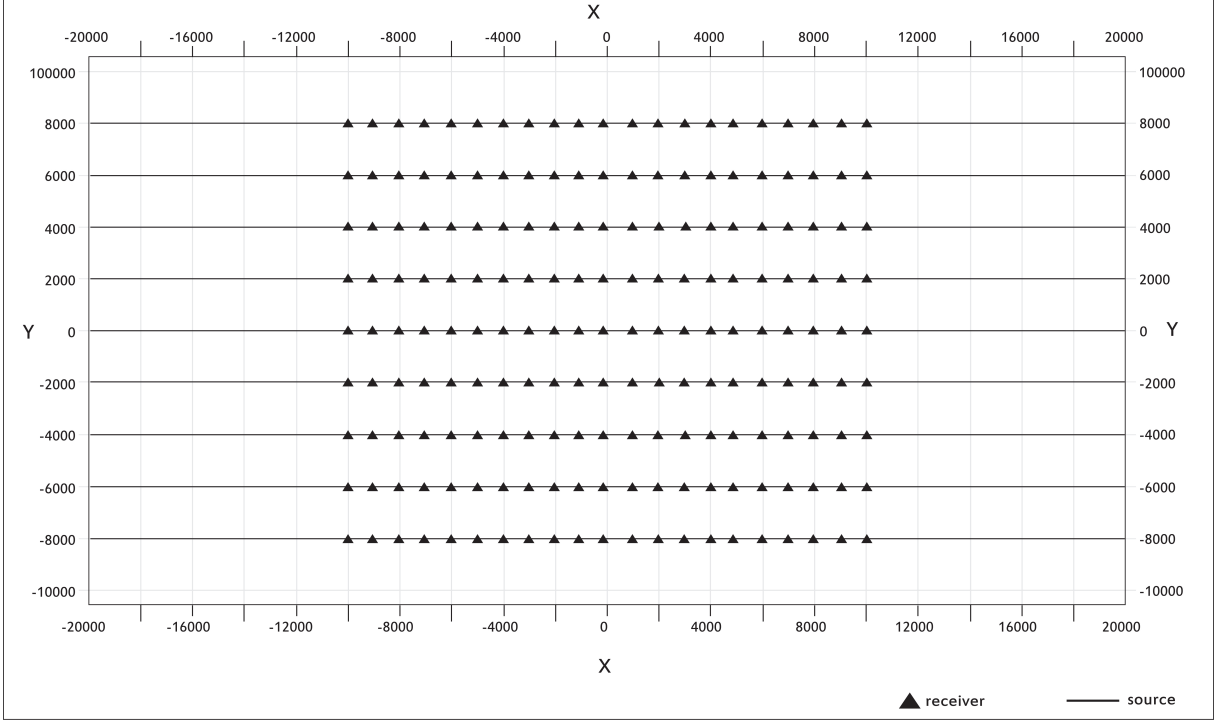


Figure 3.2: Acquisition layout for the simulated survey.

the smallest values for which a stable solution was achieved. The process reached the convergence criteria after 19 iterations.

Figure 3.3 shows a vertical section on the xz plane at $y = 0$, and figures 3.4 and 3.5 show vertical slices in the yz plane on $x = -5,500$ m and $x = -2,500$ m, respectively, with the resistivity values recovered by the inversion process. The red lines represent the positions of the resistive targets. Both bodies appear in the final section positioned approximately 250 m above the true depths. The highest resistivity recovered is 8 Ohm-m.

Figure 3.6 shows a horizontal slice at a depth of 2,200 m. The inversion has success in the delimitation of the left resistive body, albeit with overly smooth contours. The delineation of the deeper resistive body is observed in the horizontal slice at 3,150 m shown in figure 3.7. Again, a good match with the true model is achieved, with smooth borders. The highest resistivities are found at the center of the bodies, because in those regions the 1D approximation is more effective.

A measure of the data misfit for each CMP is calculated as

$$Err_{CMP} = \frac{100}{N_{obs}} \sum_{j=1}^N \left| 1 - \frac{E_{obs}}{E_{mod}} \right|. \quad (3.1)$$

The achieved overall misfit of the data is 0.45%. Figure 3.8 shows the evolution of the total data misfit with the number of the iterations. The best fit are achieved for CMPs in areas furthest from the borders of the 3D bodies, where the geometry of the true model is closer to that of a layered earth. To illustrate this behavior of the solution, figure 3.9

shows the map of misfits for all CMPs at the 3 frequencies used. The highest values in these maps are close to the positions of the borders of the resistive targets.

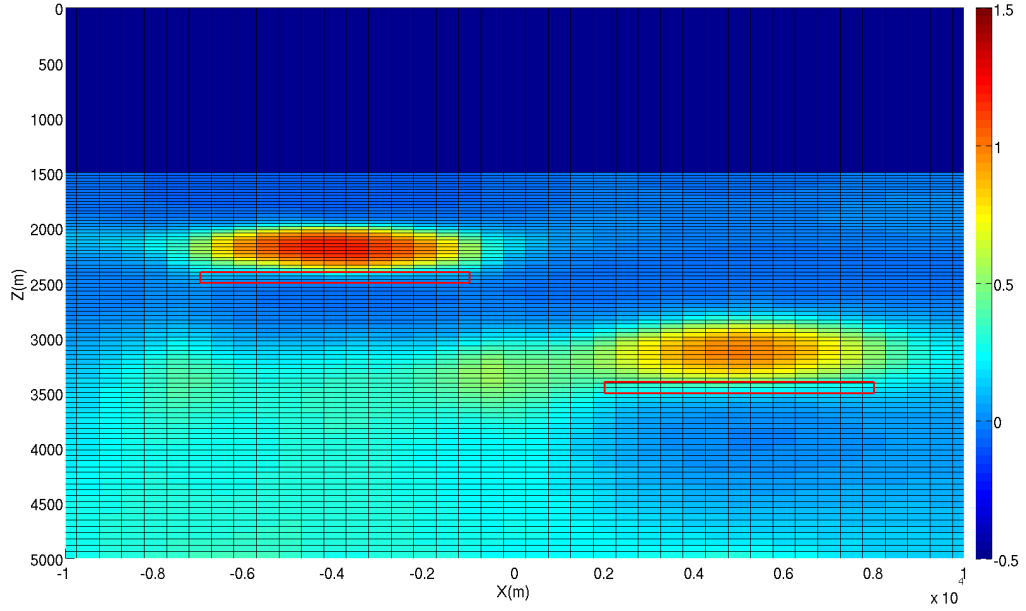


Figure 3.3: Slice XZ plane on 0 m on Y .

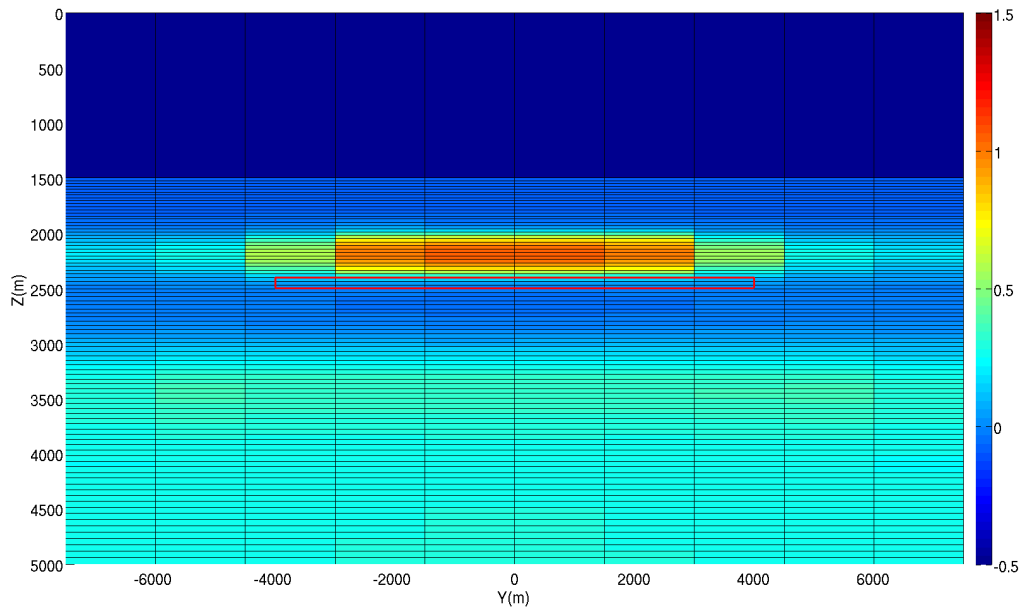


Figure 3.4: Slice YZ plane on -2500 m on X .

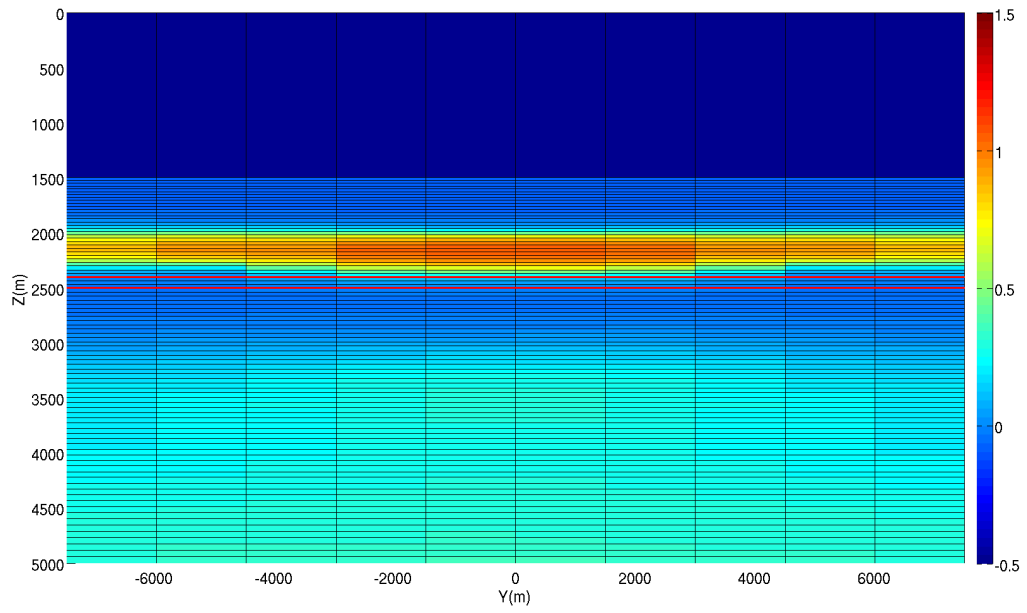


Figure 3.5: Slice YZ plane on -5500 m on X .

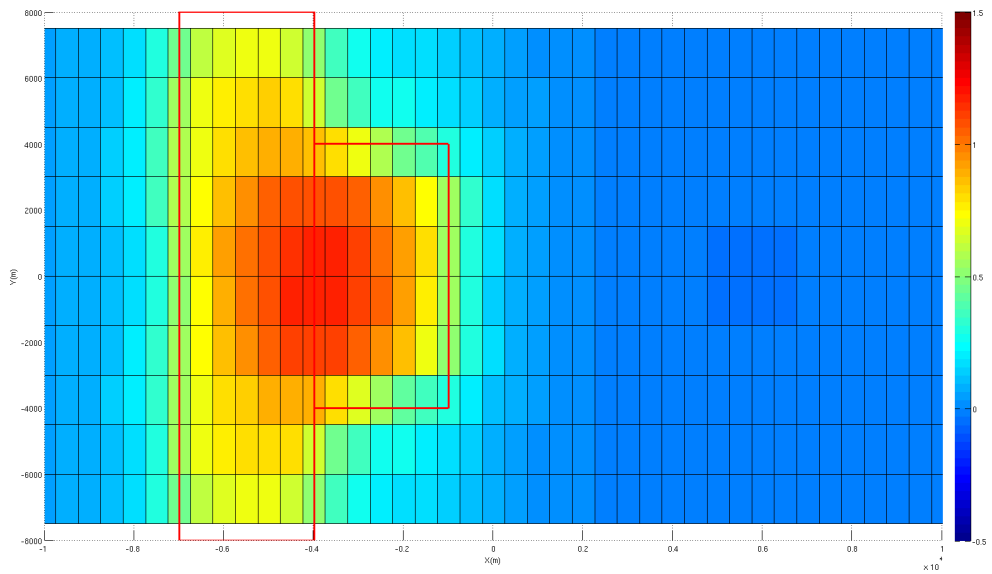


Figure 3.6: Depth slice on 2220 m.

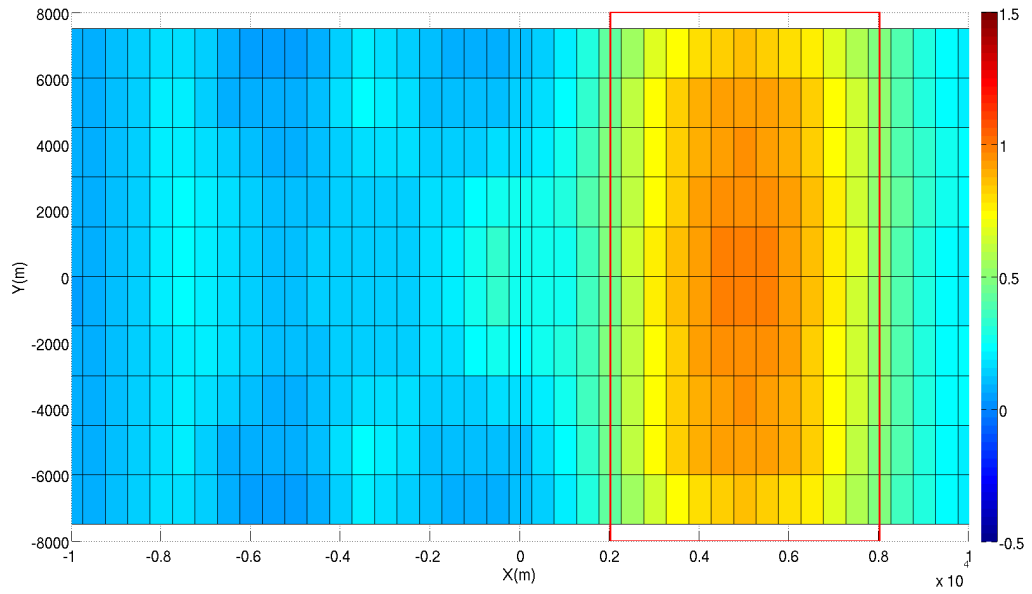


Figure 3.7: Depth slice on 3150 m.

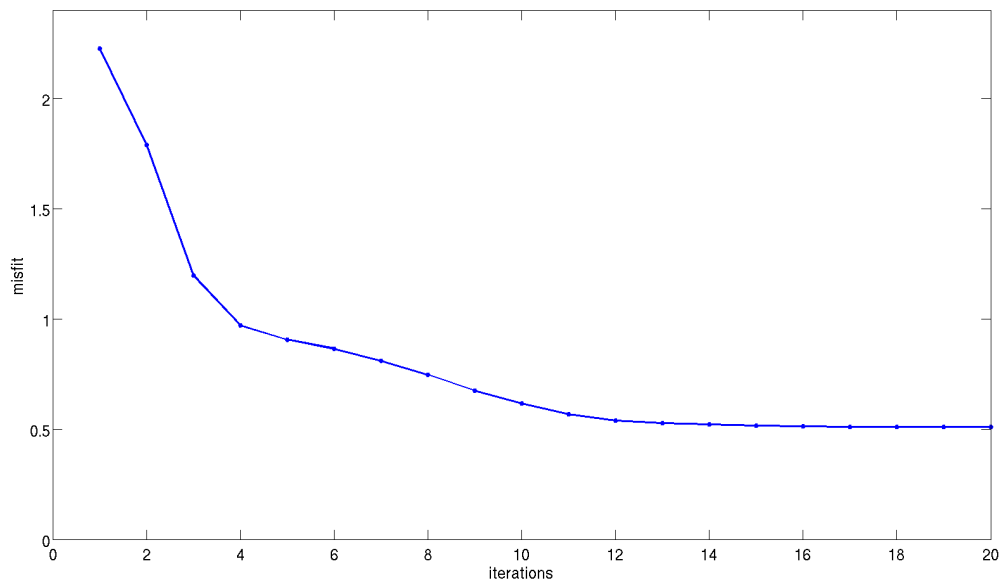
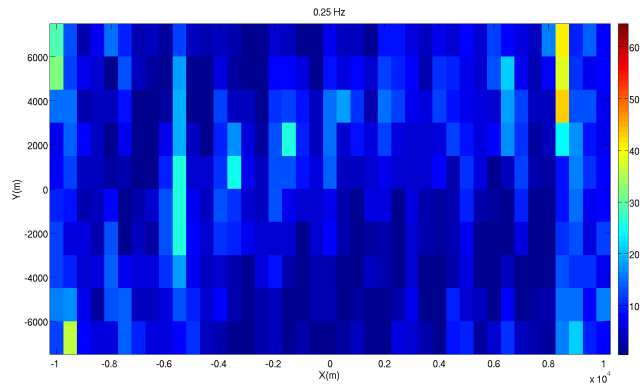
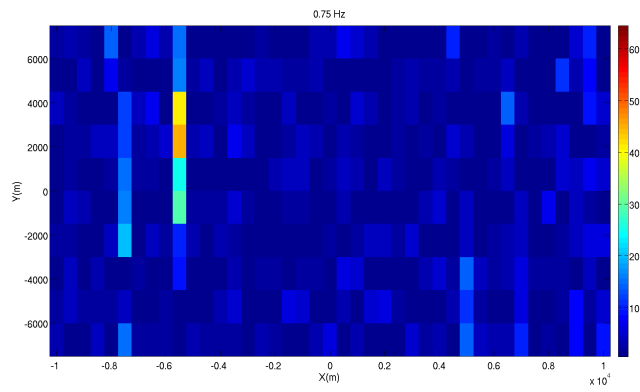


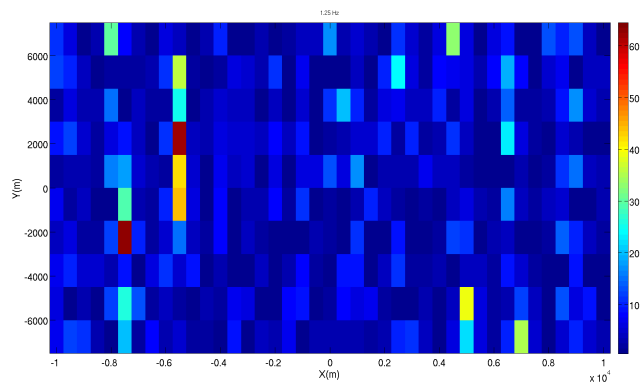
Figure 3.8: misfit



(a) 0.25 Hz



(b) 0.75 Hz



(c) 1.25 Hz

Figure 3.9: Misfit maps for the 3 frequencies used in the example.

3.1.4 Simulation of well constraint

In the exploration works, it is sometimes possible to use well logging information to drive the inversion process. In this example, it's given the information that in the true depth has a resistive region by one cell with 100 Ohm-m and 10 of weight on the a_p .

On figure 3.10 to figure 3.14 show the recovered bodies in the correct positions and with this constraint the highest resistivity recovered become 30 Ohm-m.

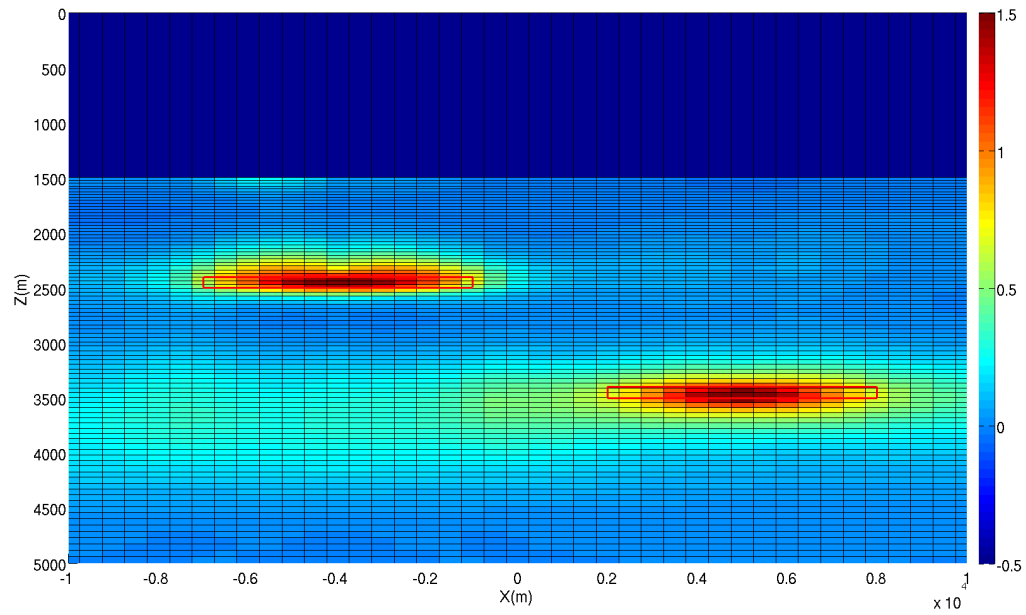


Figure 3.10: Slice XZ plane on 0 m on Y .

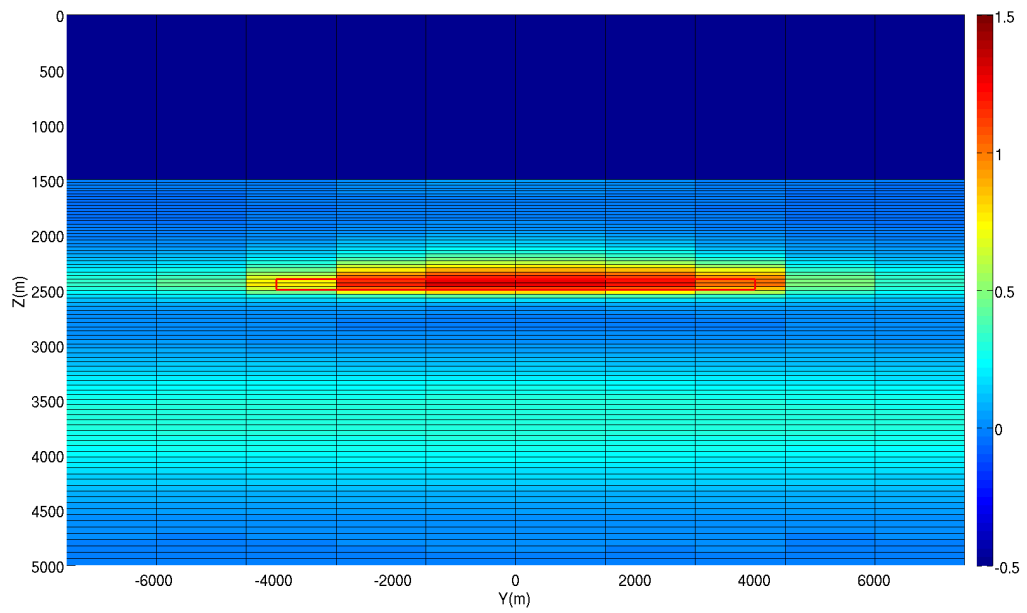


Figure 3.11: Slice YZ plane on -2400 m on X .

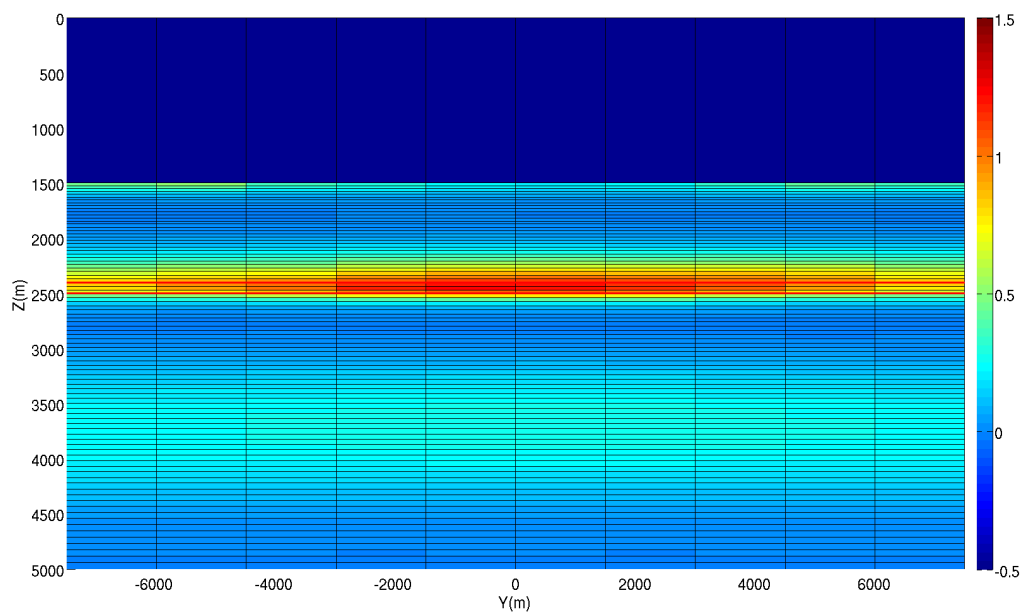


Figure 3.12: Slice YZ plane on -5500 m on X .

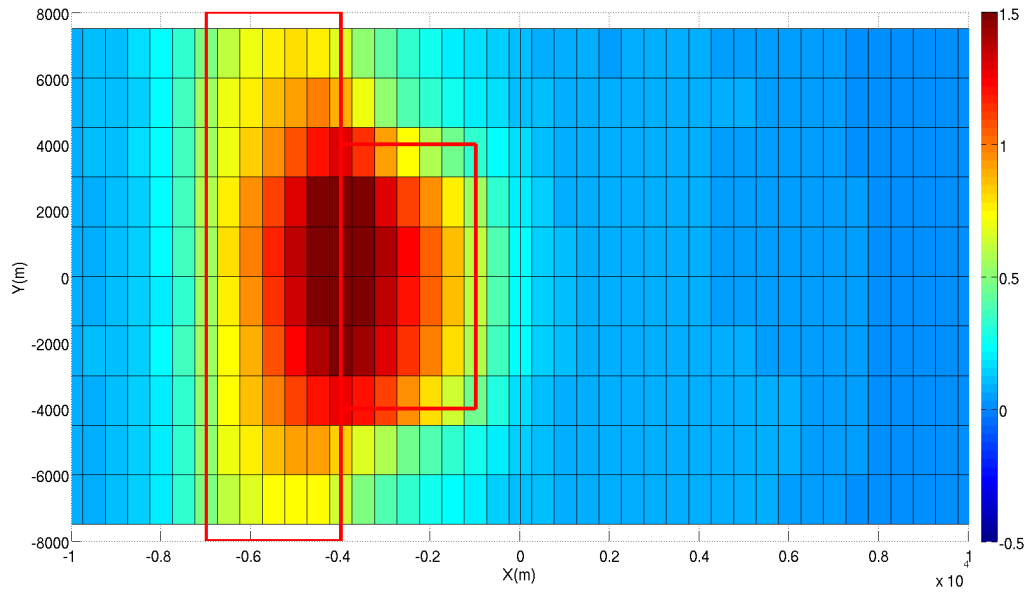


Figure 3.13: Depth slice on 2450 m.

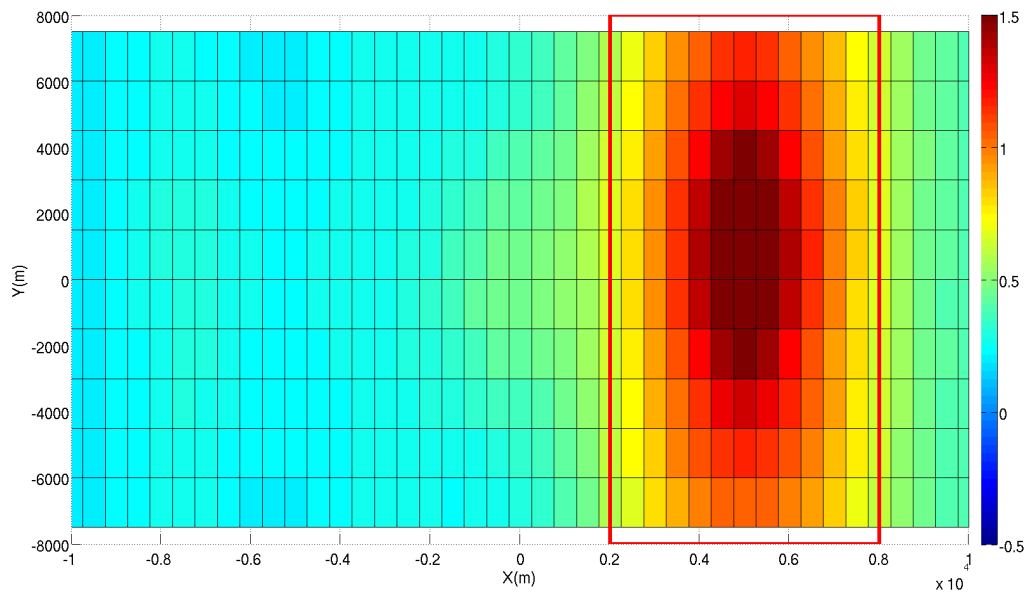


Figure 3.14: Depth slice on 3450 m.

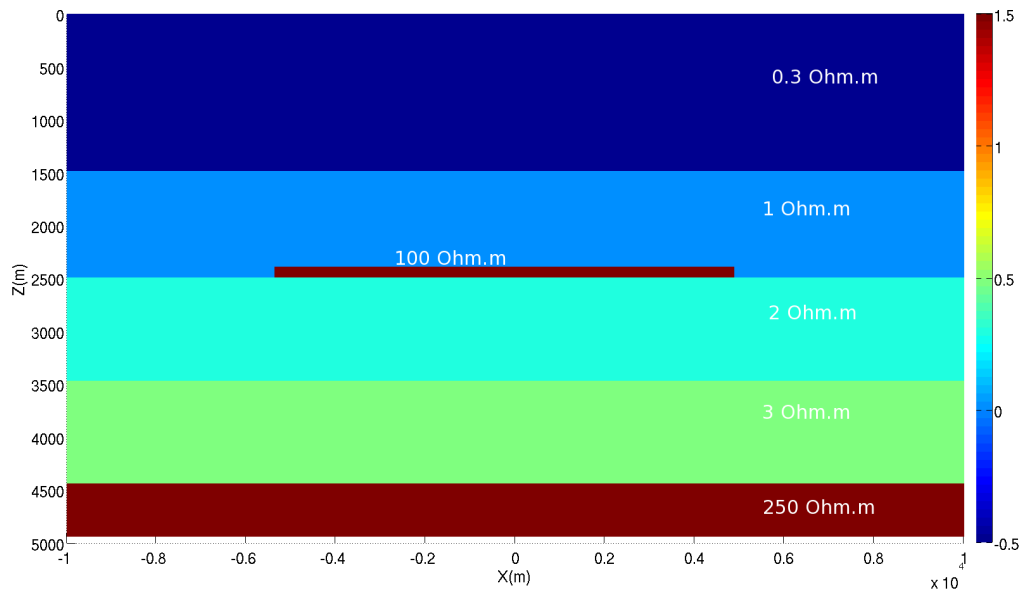
3.2 MODEL 2

The second example model is shown in figure 3.15. One resistive target (100 Ohm-m) with 100 m of thickness, at 1500m below the sea bed, is embedded in a layered model with 1, 2, 3, and 250 Ohm-m, respectively, all layers are 1 km thick.

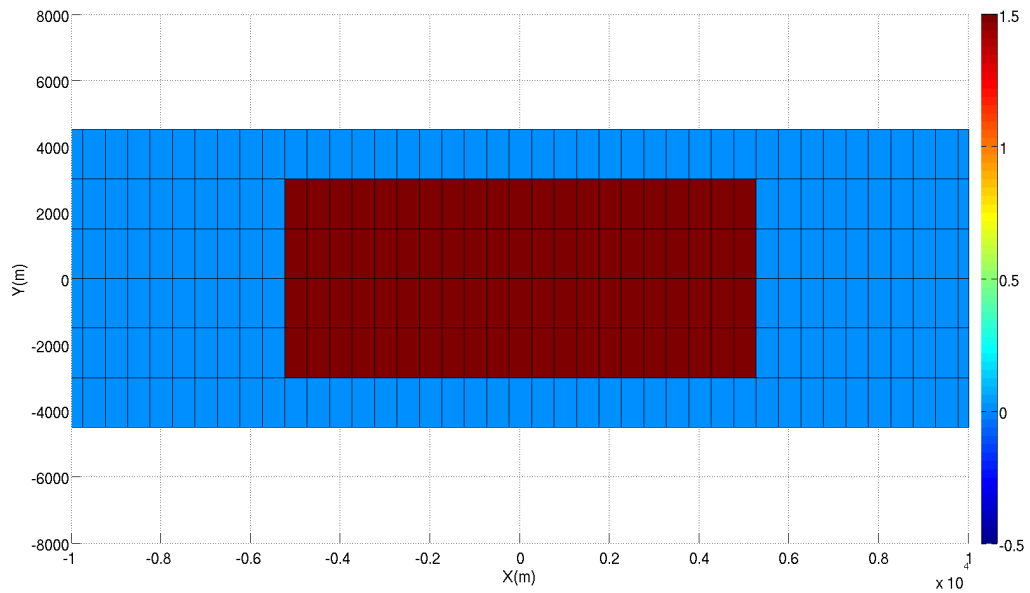
3.2.1 Inversion results 2

The same inversion grid of the first example was used, but cropped in the y direction between -4500 m to 4500 m. The resistivity start model was a homogenous layer of 1 Ohm-m from the sea bed to 4500 m and the last layer with 250 Ohm-m. This last layer was input as *a priori* information with weight of 10 on the a_p parameter.

Figure 3.16 shows a vertical section on the xz plane at $y = 0$, and figure 3.17 shows a vertical slice in the yz plane on $x = 0$ m, with the resistivity values recovered by the inversion process. The body appear in the final section well positioned in depth. The region below the body lost some sensitivity and appears with lower resistivity than the true values.



(a) Vertical section of model 2.



(b) Top view of model 2.

Figure 3.15: Model 2: 1.5 km water layer over layered sediments and a resistive target with $100\Omega\cdot\text{m}$.

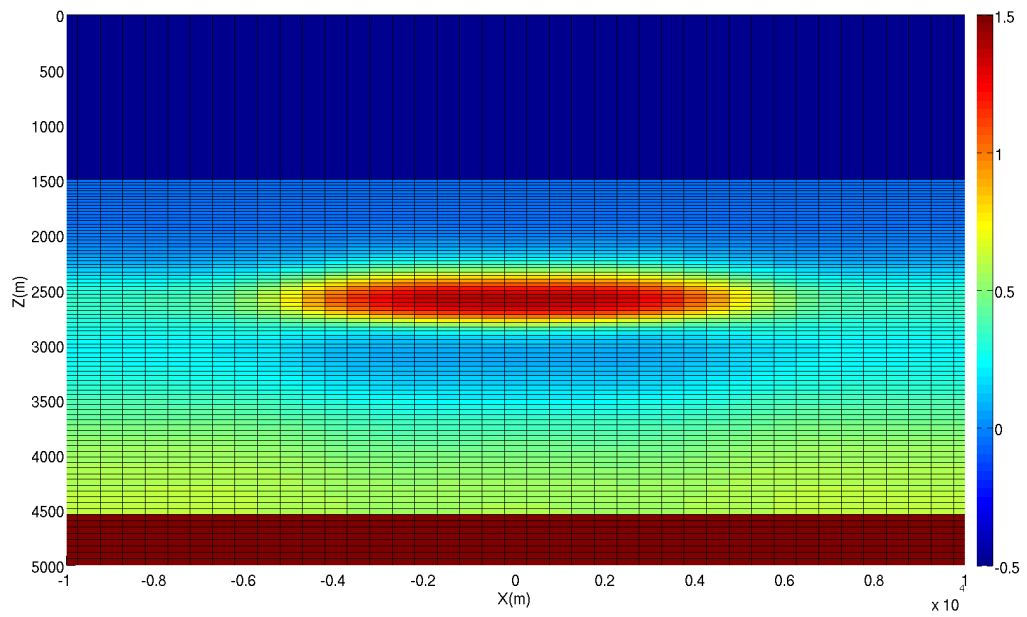


Figure 3.16: Slice XZ plane on 0 m on Y .

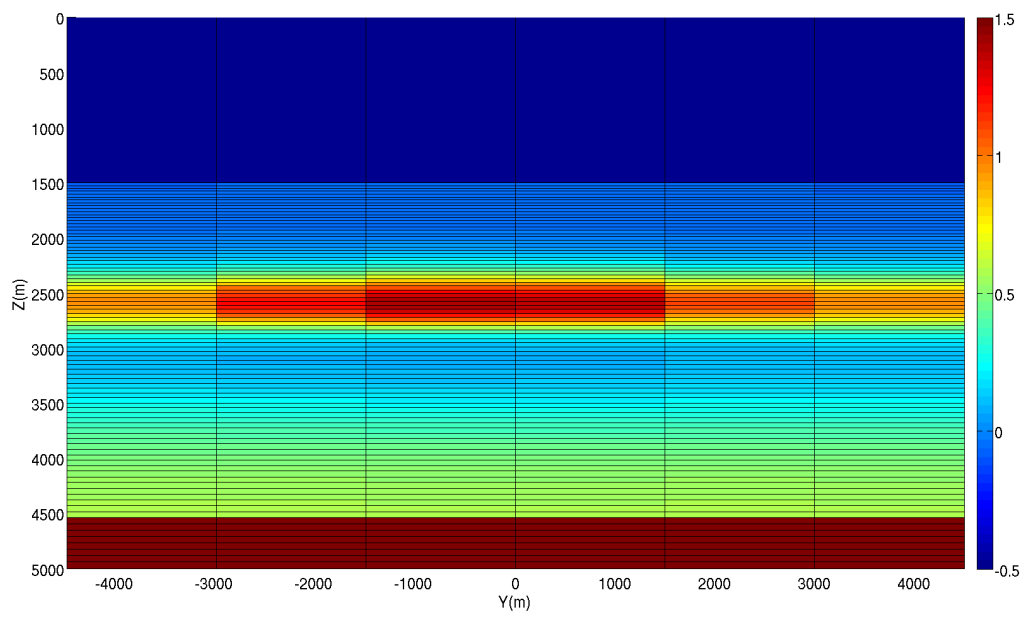


Figure 3.17: Slice YZ plane on 0 m on X .

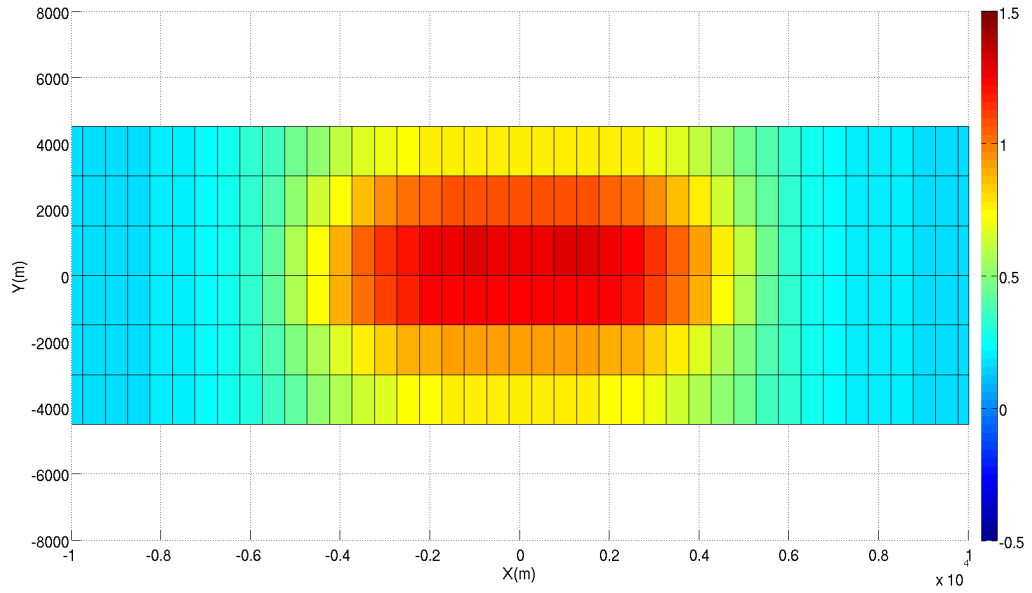
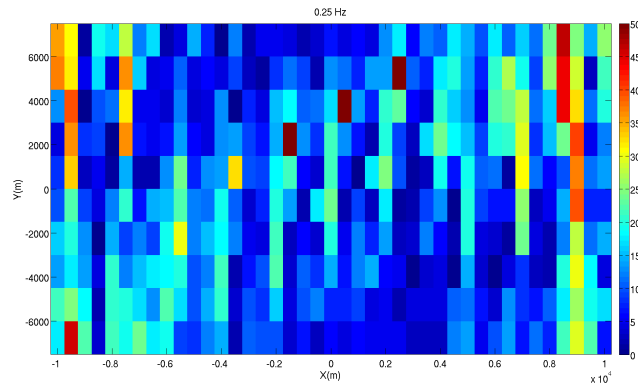
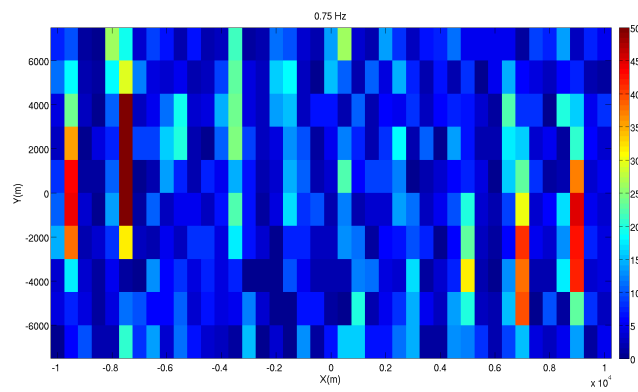


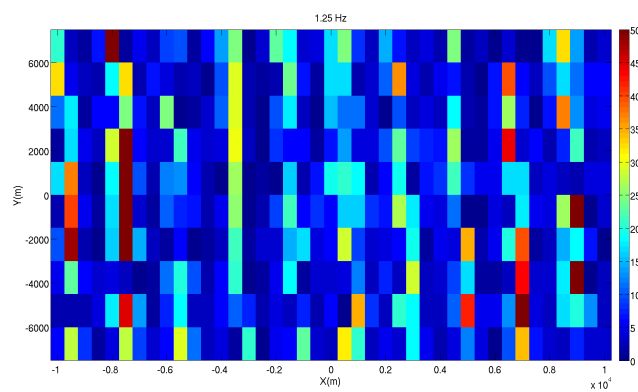
Figure 3.18: Depth slice on $z = 2500$ m.



(a) 0.25 Hz



(b) 0.75 Hz



(c) 1.25Hz

Figure 3.19: Misfit maps for the 3 frequencies used in the example.

4 FINAL REMARKS

The 1D inversion of 3D mCSEM data on the CMP domain with lateral constraints has been able to produce a quick first approximation to the geoelectrical structures under a survey area. The use of regularization constraints not only contributes to the achievement of stable solutions, but also helps to create a better delineation of the targets, by allowing the data from one CMP to exert influence on its surrounding CMP columns.

The 3D models that result from this inversion are hoped to be useful as a first interpretation tool, and also as first models in a true 3D inversion, with the possibility of saving some computer time by reducing the number of iterations.

REFERENCES

- Auken, E., and A. V. Christiansen, 2004, Layered and laterally constrained 2d inversion of resistivity data: *Geophysics*, **69**, 752–761.
- Barker, N., and D. Baltar, 2016, CSEM anomaly identification: *First Break*, **34**, 47–50.
- Buonora, M. P. P., J. L. Correa, L. S. Martins, P. T. Menezes, E. J. Pinho, J. L. Silva Crepaldi, M. P. Ribas, S. M. Ferreira, and R. C. Freitas, 2014, mCSEM data interpretation for hydrocarbon exploration: A fast interpretation workflow for drilling decision: *Interpretation*, **2**, SH1–SH11.
- Constable, S. C., R. L. Parker, and C. G. Constable, 1987, Occam’s inversion: A practical algorithm for generating smooth models from electromagnetic sounding data: *Geophysics*, **52**, 289–300.
- Crepaldi, J. L. S., M. P. P. Buonora, and I. Figueiredo, 2011, Fast marine CSEM inversion in the CMP domain using analytical derivatives: *Geophysics*, **76**, F303–F313.
- Dell’Aversana, P., and M. Vivier, 2009, Expanding the frequency spectrum in marine CSEM applications: *Geophysical Prospecting*, **57**, 573–590.
- MacGregor, L., and J. Tomlinson, 2014, Marine controlled-source electromagnetic methods in the hydrocarbon industry: A tutorial on method and practice: *Interpretation*, **2**, SH13–SH32.
- Marquardt, D. W., 1963, An algorithm for least-squares estimation of nonlinear parameters: *Journal of the society for Industrial and Applied Mathematics*, **11**, 431–441.
- Medeiros, W. E., and J. B. C. Silva, 1996, Geophysical inversion using approximate equality constraints: *Geophysics*, **61**, 1678–1688.
- Mittet, R., K. Brauti, H. Maulana, and T. A. Wicklund, 2008, CMP inversion and post-inversion modelling for marine CSEM data: *First Break*, **26**.
- Tseng, H.-W., L. MacGregor, and R. V. Ackermann, 2012, 2d inversions of 3d marine CSEM data, *in* SEG Technical Program Expanded Abstracts 2012: Society of Exploration Geophysicists, 1–5.
- Zhdanov, M. S., 2009, *Geophysical electromagnetic theory and methods*: Elsevier.